

Persistent infrared spectral hole burning of the fundamental stretching mode of SH⁻ in alkali halides

C. E. Mungan and A. J. Sievers

Laboratory of Atomic and Solid State Physics and Materials Science Center, Cornell University,
Ithaca, New York 14853-2501

Received October 10, 1991

Persistent IR spectral holes have been burned for the first time to our knowledge in the fundamental stretching mode (near 3.9 μm) of the SH⁻ molecule, matrix isolated in alkali halides, by double-doping the host with a small amount (2 mol. %) of a second alkali halide. A model is proposed for the hole-burning mechanism, involving 180° reorientations of the SH⁻ molecules between configurations rendered inequivalent by strain field gradients arising from the double-doping. The holes are found to decay within tens to hundreds of seconds at 1.5 K, implying that the barriers to the head-to-tail flips must be quite small.

1. INTRODUCTION

The technique of persistent IR spectral hole (PIRSH) burning has proved useful in elucidating the local dynamics of molecular impurities doped in alkali halide crystals.¹⁻⁵ In this paper the first observation to our knowledge of PIRSH burning of the SH⁻ diatomic in crystalline hosts is reported. This molecule is not observed to burn as an isolated impurity in KI or CsI. However, the addition of a small (~2 mol. %) amount of a second alkali halide is found to destroy the local symmetry around some of the SH⁻ molecules, thus broadening the main vibrational stretching band in an inhomogeneous manner as well as creating a new mode that is assigned to a SH⁻:ion combination, where the ion in question is either a foreign alkali or halide ion that substitutes for a host ion on one of the nearest allowed sites. This new mode, as well as the low-frequency wing of the broadened main band, are now found to exhibit PIRSH burning. By studying the properties of the resulting holes and antiholes, new information about the SH⁻ defect is obtained.

The organization of the paper is as follows. First the experimental hole-burning setup and sample preparation are described. Next, Fourier transform infrared (FTIR) absorption spectra and hole-burning data are presented for SH⁻ doped in KI and CsI host crystals. Finally the PIRSH burning results are compared with previous findings for ReO₄⁻ hole burning¹ in strained KI and RbI crystals and for CN⁻ hole burning⁵ in KBr:NaBr, and a possible model for the hole-burning mechanism is discussed.

2. EXPERIMENTAL DETAILS

The experimental setup used for hole burning is similar to that described in Ref. 5. Basically, a cw PbEuSeTe striped double-heterojunction diode laser (DL), temperature and current tunable over the range 2322–2607 cm^{-1} , is focused onto the input of a 1/2-m monochromator. The monochromator selects one line out of the five or so modes output by the DL and calibrates that line's frequency to within ~1 cm^{-1} . The exact frequency is determined by

observing the transmission at a known, sharp feature in some sample, such as a SH⁻ stretching vibrational mode. The useful continuous tuning range of the DL is limited to ~1/2 cm^{-1} because of the tendency of the laser to mode hop. A 2.54-cm germanium étalon is used to calibrate the actual frequency range of the laser sweep (in gigahertz) and to check for incoherent or closely spaced multi-mode output from the DL. The laser beam is principally vertically polarized; however, a 5.3- μm CdS half-wave plate and a ZnSe Brewster-angle polarizer are used to select other desired polarizations.

After the monochromator the beam is focused onto a sample held in an optical-access cryostat at 1.5 K; the cryostat has sapphire inner and CaF₂ outer windows. The spot size at the sample is measured as having a FWHM of 75 μm at the sample, when a Gaussian transverse beam profile is assumed, and a power meter is used to measure the maximum incident laser power (depending on the exact frequency) of 90 μW just before the cryostat. After correction for reflection losses at the windows, these imply an incident intensity as high as 2 W/cm^2 at the sample position. Lower incident intensities are obtained by inserting neutral-density filters into the beam. Finally, the transmission through the sample is detected by using a 77-K InSb photovoltaic detector and is recorded by a digital storage oscilloscope under computer control.

The SH⁻-doped alkali halide samples were grown by the Czochralski method at Cornell's Materials Science Center. Special precautions were taken to purify and dry the starting materials. The samples were characterized before the hole-burning measurements by using a FTIR interferometer operating at a resolution of 0.04 cm^{-1} . The actual SH⁻ concentration in a given sample can be determined from the integrated absorption cross section⁶ at RT:

$$\int \alpha d\nu/N = 1.11 \times 10^{-18} \text{ cm} \pm 20\%, \quad (1)$$

where ν is the frequency in inverse centimeters, $\alpha(\nu)$ is the absorption coefficient in inverse centimeters, and N is the defect concentration per cubic centimeter. This value for

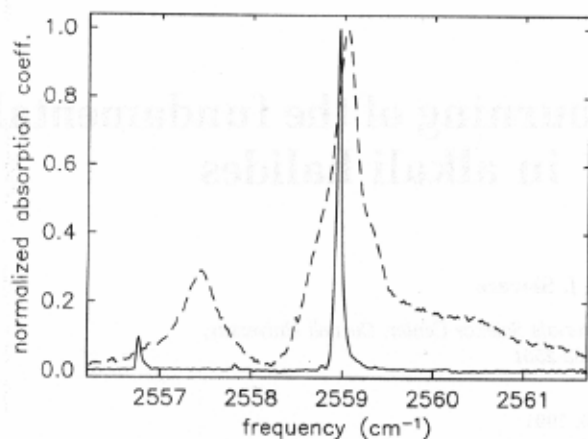


Fig. 1. Comparison of the FTIR absorption spectra at a 0.04-cm^{-1} resolution and 1.5 K of nominally KI + 0.006 mol. % KSH (solid curve) and KI + 2 mol. % KBr + 0.02 mol. % KSH (dashed curve) in the region of the fundamental SH^- stretching mode. The vertical scale on each curve has been adjusted to give a peak value (for the $^{32}\text{SH}^-$ absorption band) of unity; the actual peak absorption coefficients are listed in Table 1 along with the center frequencies and FWHM's of the observed features.

Eq. (1) was obtained by first measuring and integrating the absorption spectra of several nominally KI + 0.2 mol. % KSH samples and then dividing these integrals by the actual SH^- concentrations of the respective samples, as determined by using the chemical analysis technique of Ref. 7. It is assumed that this integrated cross section is host independent to within the quoted error.

3. EXPERIMENTAL RESULTS

A. KI Host Samples

1. Fourier Transform Infrared Spectra

In Fig. 1 the FTIR absorption spectrum of a sample of nominally KI + 0.006 mol. % KSH (solid curve) is compared with that of nominally KI + 2 mol. % KBr + 0.02 mol. % KSH (dashed curve) at 1.5 K. The actual SH^- concentrations (N), center frequencies (ν_1), peak absorption coefficients (α_{peak}), and FWHM of the features observed in these spectra are tabulated in the upper half of Table 1. Sulfur has four naturally occurring isotopes:

^{32}S (95.0% natural abundance), ^{33}S (0.76%), ^{34}S (4.22%), and ^{36}S (0.02%, too small to observe). With the assumption of an isolated harmonic oscillator model for the internal stretching vibration of the SH^- molecule, the center frequency ν_1 of a given line is proportional to the reciprocal of the square root of the reduced mass, $\mu = m_{\text{S}}m_{\text{H}}/(m_{\text{S}} + m_{\text{H}})$, where m_{S} and m_{H} are the atomic masses of the sulfur isotope and of hydrogen, respectively. One would also expect the FWHM to be constant for the different isotopes and expect the peak absorption coefficient α_{peak} to scale with the natural isotopic abundance. Using the values of ν_1 and α_{peak} for $^{32}\text{SH}^-$ (see Table 1), one thus predicts, for KI + 60 parts in 10^6 KSH,

$$\nu_1(^{34}\text{SH}^-) = 2556.67\text{ cm}^{-1},$$

$$\nu_1(^{33}\text{SH}^-) = 2557.84\text{ cm}^{-1},$$

$$\alpha_{\text{peak}}(^{34}\text{SH}^-) = 0.39\text{ cm}^{-1},$$

$$\alpha_{\text{peak}}(^{33}\text{SH}^-) = 0.070\text{ cm}^{-1}.$$

These values are in approximate agreement with the tabulated numbers. The three lines observed in KI + 60 parts in 10^6 KSH are therefore assigned to the stretching modes of the three main isotopes of SH^- , as listed in the last column of Table 1. The two lower-frequency lines were incorrectly identified as SH^- cluster modes in previous studies of the IR spectra (see, for example, Ref. 7), in part because of insufficient spectrometer resolution.

When Br^- atoms are additively doped into the sample (see Fig. 1), the main $^{32}\text{SH}^-$ line broadens asymmetrically, and a new band appears between the $^{34}\text{SH}^-$ and the $^{33}\text{SH}^-$ frequency locations. The most likely origin of this new band is absorption by $^{32}\text{SH}^-$ centers perturbed by the presence of a single Br^- ion sitting on one of the twelve nearest anionic sites, that is to say, a second-nearest neighbor (2nn) to the SH^- in any one of the twelve $\langle 110 \rangle$ directions. One would expect such a perturbation to shift the $^{32}\text{SH}^-$ vibration to slightly lower frequencies because of the enlarged lattice cavity in which the defect resides, owing to the smaller ionic radius of Br^- compared with that of I^- . A simple statistical estimate confirms this assignment: There is a 2% chance that any given I^- site will be occupied instead by Br^- (with a fully random

Table 1. Characteristics of the FTIR Spectral Features in Figures 1 and 5^a

Sample	N (ppm)	ν_1 (cm^{-1})	α_{peak} (cm^{-1})	FWHM (cm^{-1})	Assignment
KI + 60 parts in 10^6 KSH	88	2556.77	0.85	0.038	$^{34}\text{SH}^-$
		2557.83	0.16	0.038	$^{33}\text{SH}^-$
		2558.95	8.7	0.043	$^{32}\text{SH}^-$
KI + 2% KBr + 0.02% KSH	150	2557.43	0.65	0.52	$^{32}\text{SH}^-:\text{Br}^-$
		2559.04	2.3	0.50	$^{32}\text{SH}^-$
CsI + 75 parts in 10^6 KSH	66	2533.17	0.32	0.028	$^{34}\text{SH}^-$
		2534.21	0.06	0.028	$^{33}\text{SH}^-$
		2535.32	3.2	0.030	$^{32}\text{SH}^-$
CsI + 2% RbI + 0.05% KSH	840	2533.20	0.55	0.23	$^{34}\text{SH}^-$
		2534.23	0.04	0.07	$^{33}\text{SH}^-$
		2534.70	1.2	0.20	$^{32}\text{SH}^-:\text{Rb}^+$
		2535.35	10.3	0.23	$^{32}\text{SH}^-$

^aThe first column gives the nominal sample concentrations; the second the actual SH^- concentration N determined by using Eq. (1); the third the center frequency ν_1 of the band in question; the fourth its peak absorption coefficient α_{peak} ; the fifth its FWHM (after deconvolving the 0.04-cm^{-1} resolution of the FTIR in quadrature); and the sixth its assignment, as discussed in the text.

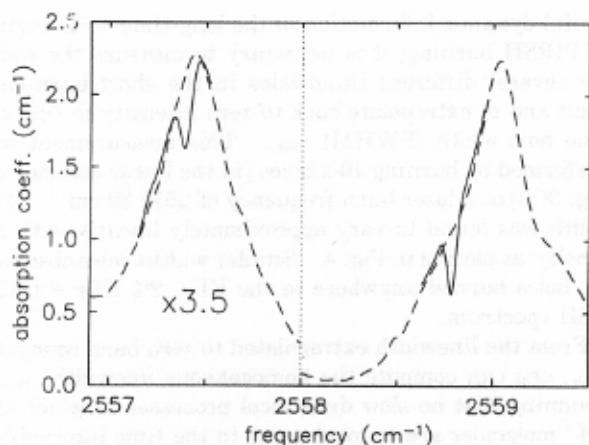


Fig. 2. Two holes separately burned in the $^{32}\text{SH}^-:\text{Br}^-$ band (left-hand side, enlarged vertically by a factor of 3.5, as indicated) and in the main $^{32}\text{SH}^-$ vibrational mode (right-hand side). The dashed curves are the original, unburned FTIR spectra from Fig. 1, and the solid curves show the spectra resulting from burning at 2557.39 cm^{-1} for 2 min at 1 W/cm^2 (left-hand side) and at 2558.78 cm^{-1} for 1 min at 0.8 W/cm^2 (right-hand side).

distribution of Br^- ions in the lattice), and hence the probability of finding one 2nn site occupied by Br^- relative to that of finding none so occupied is $12 \times 0.02/0.98 = 0.24$. This agrees with the ratio of the areas of the 2557.43-cm^{-1} (neglecting the underlying $^{34}\text{SH}^-$ and $^{33}\text{SH}^-$ lines) and the 2559.04-cm^{-1} bands, which is found by integration to be 0.24. Similarly, the broadening of the main $^{32}\text{SH}^-$ mode may arise from Br^- ions sitting on anionic sites further removed than 2nn from the defect, 4nn for example, with a consequently smaller influence on the stretching frequency.

2. Hole Burning

Attempts were made to burn holes in both the singly doped and the doubly doped samples at the various absorption features shown in Fig. 1. No holes were observed in the singly doped sample; however, for the doubly doped sample, holes could be burned in the $^{32}\text{SH}^-:\text{Br}^-$ band and on the low-frequency side of the asymmetric main line. In Fig. 2 an example of a hole (solid curve, left-hand side) burned for 2 min at 2557.39 cm^{-1} and 1 W/cm^2 is plotted on top of the unburned spectrum (dashed curve), and, from a separate run (right-hand side), at 2558.78 cm^{-1} for 1 min at 0.8 W/cm^2 . The antiholes are clearly visible as regions of increased absorption beyond the wings of the holes, peaking on average at $\sim 4\text{-GHz}$ -higher and -lower frequencies. It is impossible to determine whether all the area of these holes is accounted for by their respective antihole absorption strengths because of inadequate signal-to-noise resolution and single-mode DL frequency sweep range. At these intensities the maximum observed hole depth in absorption was $\sim 50\%$. Furthermore the holes decayed within a matter of minutes [see Fig. 3(a)]. Hence the barrier between the original and the burned configurations must be quite small, and the relaxation undoubtedly competes with the burning efficiency, so that 100%-deep holes are not obtained.

The decay of a 3-min hole in transmission, burned in the $\text{SH}^-:\text{Br}^-$ band at 2557.20 cm^{-1} with a 500-mW/cm^2 incident intensity, is plotted in Fig. 3(a). The filled circles

show the decay that occurs when the hole is continuously monitored by repetitively sweeping the laser frequency over the hole spectrum. The solid line is a fit to an exponential with a $1/e$ decay time τ of 73 s. However, it was found that the probe laser itself contributes to the decay: Blocking the laser after burning the hole and waiting for some time before probing the spectrum, then repeating these steps for other waiting times, reveals that the unprobed hole [filled squares in Fig. 3(a)] decays with a $1/e$ time τ' (dashed line) of only 260 s. Apparently the probe laser contributes a second exponential decay with a time constant τ'' , so that $1/\tau = 1/\tau' + 1/\tau''$, with $\tau'' = 100\text{ s}$. Such an effect was seen previously¹ for the laser-induced decay of PIRSH's burned in ReO_4^- . Unfortunately it was not possible to attenuate the probe beam after burning a hole because of the tiny spot size and consequent high sensitivity of the spectrum to minute deflections of the laser. However it appears that the slow decay (τ') is intrinsic to the relaxation dynamics of the SH^- molecule in the host; note in particular that the cold sapphire windows on the

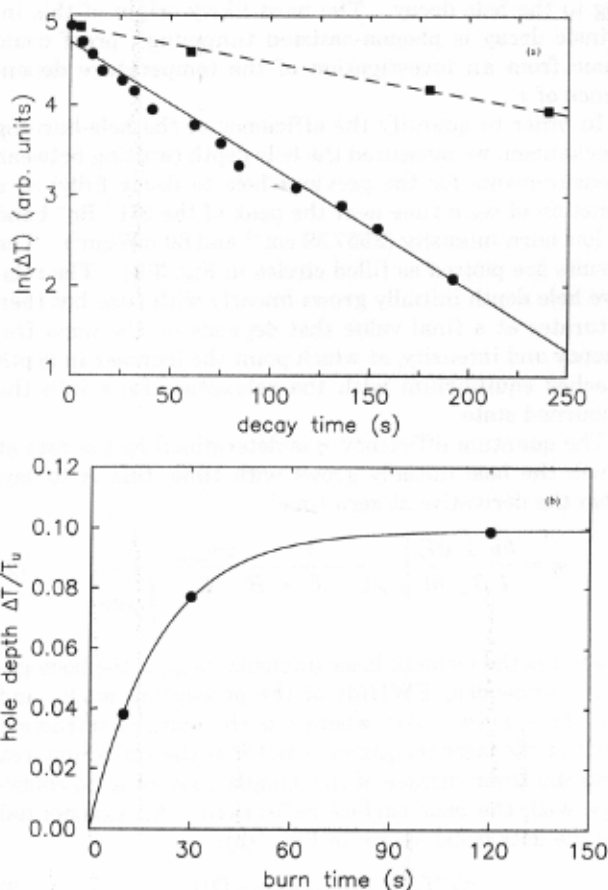


Fig. 3. (a) Decay of a hole burned for 3 min at 2557.20 cm^{-1} and 500 mW/cm^2 as measured by continuously sweeping the laser over the spectrum (filled circles) and by waiting for some time before probing the hole (filled squares, each point measured starting from a fresh hole). The vertical axis is the natural logarithm of the hole depth in transmission $\Delta T \equiv T_b - T_u$, where T_b is the burned and T_u the unburned transmissions of the sample (in arbitrary units). The lines are best fits to an exponential: $\Delta T = \Delta T_0 \exp(-t/\tau)$, where $\Delta T_0 = 110$ and $\tau = 73\text{ s}$ for the solid line, and $\Delta T_0 = 130$ and $\tau = 260\text{ s}$ for the dashed line. (b) Growth of a hole (filled circles) as a function of burn time at 2557.39 cm^{-1} and 60 mW/cm^2 burn intensity. The solid curve is a fit to Eq. (3), with $A = 0.0993$ and $\Gamma = 0.0492\text{ s}^{-1}$.

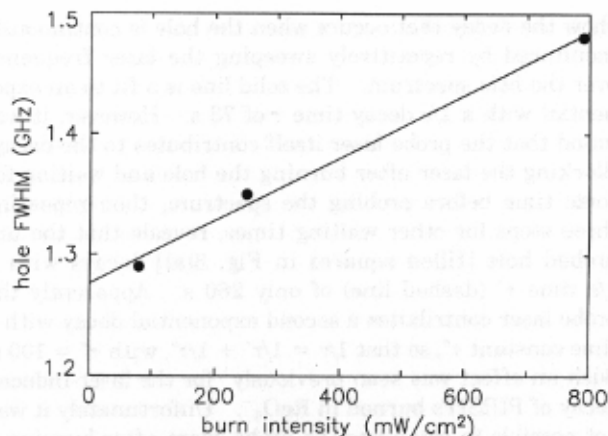


Fig. 4. Hole width (FWHM) as a function of burn intensity I for 10-s burns at 2557.39 cm^{-1} (filled circles). The solid line is a least-squares fit to the data: $1.276 \text{ GHz} + (2.61 \times 10^{-4} \text{ GHz cm}^2/\text{mW}) \times I$.

cryostat filter out most of the RT blackbody background radiation, so that this background should not be contributing to the hole decay. The most likely origin of this intrinsic decay is phonon-assisted tunneling⁶; proof could come from an investigation of the temperature dependence of τ' .

In order to quantify the efficiency of the hole-burning mechanism, we measured the hole depth (waiting between measurements for the previous hole to decay fully) as a function of burn time near the peak of the $\text{SH}^-:\text{Br}^-$ band at low burn intensity (2557.39 cm^{-1} and 60 mW/cm^2). The results are plotted as filled circles in Fig. 3(b). The relative hole depth initially grows linearly with time but then saturates at a final value that depends on the burn frequency and intensity, at which point the increase in depth reaches equilibrium with the relaxation back into the unburned state.

The quantum efficiency η is determined by the rate at which the hole initially grows with time, that is to say, from the derivative at zero time¹:

$$\eta = \frac{h\nu}{I} \frac{1}{T_u} \left. \frac{dT_b}{dt} \right|_{t=0} \frac{1}{1 - T_u - R} \frac{\pi\gamma_{\text{homo}}}{2} \frac{N}{\int \alpha d\nu}, \quad (2)$$

where I is the incident laser intensity, γ_{homo} is the homogeneous linewidth (FWHM) of the absorption mode, and $R = [(n-1)/(n+1)]^2$, where n is the index of refraction of KI at the laser frequency ν and R is the reflection loss from the front surface of the sample (assuming no coherence with the back-surface reflection). An exponential fits the data (solid curve) in Fig. 3(b):

$$\Delta T/T_u = A[1 - \exp(-\Gamma t)], \quad (3)$$

where $\Delta T \equiv T_b - T_u$ is the hole depth in transmission; T_u and T_b are the unburned and burned sample transmissions, respectively, so that the slope at zero time, $dT_b/T_u dt|_{t=0}$, is $A\Gamma$. Inserting the appropriate values into Eq. (2) [γ_{homo} is obtained using Eq. (4) below], one finds that $\eta = 5.9 \times 10^{-4}$, that is to say, ~ 1 in every 1700 photon absorptions induces a center to burn.

As is well known,⁹ the width of a PIRSH depends on the incident burn intensity and burn time as a result of power broadening and sample heating. Thus, in order to extract

useful dynamic information in the long-time-scale regime of PIRSH burning, it is necessary to measure the width for several different intensities in the short-burn-time limit and to extrapolate back to zero intensity to find the true hole width (FWHM) γ_{hole} . This measurement was performed by burning 10-s holes [in the linear regime; see Fig. 3(b)] at a laser burn frequency of 2557.39 cm^{-1} . The width was found to vary approximately linearly with intensity, as plotted in Fig. 4. Similar widths were observed for holes burned anywhere in the KI + 2% KBr + 0.02% KSH spectrum.

From the linewidth extrapolated to zero burn intensity, γ_{hole} , one can compute the homogeneous linewidth, γ_{homo} , assuming that no slow dynamical processes to which the SH^- molecules are coupled occur in the time interval between hole burning and observation¹⁰; γ_{homo} is related in turn to the total dephasing time T_2 according to¹¹

$$\gamma_{\text{hole}} = 2\gamma_{\text{homo}} = \frac{2}{\pi T_2} = \frac{1}{\pi T_1} + \frac{2}{\pi T_2^*}, \quad (4)$$

where T_1 is the energy relaxation time and T_2^* is the pure dephasing time. Assuming that the former dominates, i.e., $T_1 \ll T_2^*$, one can calculate T_1 from the hole width, obtaining 250 ps for SH^- in KI + 2% KBr and 370 ps for SH^- in CsI + 2% RbI. These results are in excellent agreement with values for the energy relaxation time obtained directly from measurements of the incoherent saturation intensity.¹²

Measurements of the polarization dependence of the PIRSH's were performed, with the following results. A hole was burned with [100] polarized light incident on a [100]-cleaved crystal. The resulting spectrum was then probed under both [100] and [010] polarizations. In both cases the hole and antihole could be seen, and the hole depths were approximately equal for the two probe polarizations, as were the antihole heights. Next a fresh hole was burned with [110] polarization and probed with [110] and $[\bar{1}\bar{1}0]$ polarized light. In this case the hole and antihole were both found to be strongly polarized in the [110] orientation, with a weak residual [110] spectrum, which is probably a result of the imperfect efficiencies of the half-wave plate and the Brewster-angle polarizer. It should be remarked that identical polarization dependences were found for holes burned anywhere in the KI + 2% KBr + 0.02% KSH spectrum. In particular, no difference was found for holes burned in the $\text{SH}^-:\text{Br}^-$ band compared with those burned in the main SH^- line.

B. CsI Host Samples

Cesium iodide has a different crystal structure than does potassium iodide. Consequently PIRSH's were also burned in CsI to reveal how its structure influences the hole properties.

1. Fourier Transform Infrared Spectra

In Fig. 5 the FTIR absorption spectrum of a sample of nominally CsI + 0.0075 mol. % KSH (solid curve) is plotted on top of that of nominally CsI + 2 mol. % RbI + 0.05 mol. % KSH (dashed curve) at 1.5 K. The actual SH^- concentrations and center frequencies, peak absorption coefficients, and FWHM of the observed features in these spectra are tabulated in Table 1 (lower half). In this case the harmonic oscillator model predicts for

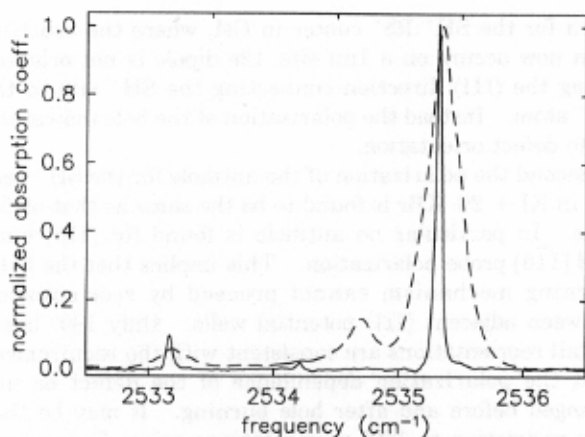


Fig. 5. Comparison of the FTIR absorption spectra at a 0.04-cm^{-1} resolution and 1.5 K of nominally CsI + 0.0075 mol. % KSH (solid curve) and CsI + 2 mol. % RbI + 0.05 mol. % KSH (dashed curve) in the region of the fundamental SH^- stretching mode. The vertical scale on each curve has been adjusted to give a peak value (for the $^{33}\text{SH}^-$ absorption band) of unity; the actual peak absorption coefficients are listed in Table 1 along with the center frequencies and FWHM of the observed features.

CsI + 75 parts in 10^6 KSH that

$$\begin{aligned}\nu_1(^{34}\text{SH}^-) &= 2533.09\text{ cm}^{-1}, \\ \nu_1(^{33}\text{SH}^-) &= 2534.25\text{ cm}^{-1}, \\ \alpha_{\text{peak}}(^{34}\text{SH}^-) &= 0.44\text{ cm}^{-1}, \\ \alpha_{\text{peak}}(^{33}\text{SH}^-) &= 0.080\text{ cm}^{-1},\end{aligned}$$

again confirming the assignment of the three observed lines to the stretching modes of the main SH^- isotopes.

The addition of Rb^+ atoms into the melt (see Fig. 5) causes the main line to broaden asymmetrically and a new line to appear at 2534.70 cm^{-1} , between the $^{33}\text{SH}^-$ and $^{32}\text{SH}^-$ modes. This new line is assigned to absorption from a $^{32}\text{SH}^-$ center with a single Rb^+ ion substituted at one of its nearest cationic sites, or in other words, a first-nearest neighbor (1nn) to the SH^- in one of the eight $\langle 111 \rangle$ directions. Since there is a 2% chance that any given Cs^+ site is occupied instead by Rb^+ (assuming that the presence of a given Rb^+ or SH^- ion does not influence the probability for Rb^+ atoms to substitute at neighboring sites), it follows that the probability of finding one 1nn site occupied by Rb^+ relative to that of finding none is $8 \times 0.02/0.98 = 0.16$. This value can be compared with the ratio of the areas of the 2534.70 cm^{-1} and the 2535.35 cm^{-1} lines, which is found by fitting the sum of two Lorentzians to the spectrum, to be ~ 0.10 , in reasonable agreement. (The peak frequencies, widths, and heights of these two lines, as listed in Table 1, were obtained from this fit.)

2. Hole Burning

No hole burning was observed to occur anywhere in the CsI + 75 parts per 10^6 KSH spectrum in Fig. 5. However, for the doubly doped sample, holes could be burned in the $^{32}\text{SH}^-:\text{Rb}^+$ and on the low-frequency side of the main $^{32}\text{SH}^-$ line. Figure 6 shows examples of holes burned (in separate runs) for 1 min at 2 W/cm^2 into the spectrum of CsI + 2% RbI + 0.05% KSH at the following frequencies: 2534.81 , 2534.89 , 2535.01 , and 2535.16 cm^{-1} . The in-

creased absorption in the wings of each hole indicates the edges of the antiholes; however, these wings could not be clearly followed further in frequency because of the presence of several nearby laser modes output by the DL in this region of operation. Note how shallow the holes are (expanded by a factor of 37 relative to the FTIR spectrum in Fig. 6); the maximum observed hole depth in absorption was only $\sim 12\%$. This shallowness may be explained in part by the fact that these holes were found to decay significantly faster ($1/e$ decay time $\approx 15\text{ s}$ in the dark) than those burned in KI + 2% KBr + 0.02% KSH. The hole FWHM in the low-intensity limit is $\sim 860\text{ MHz}$, to within approximately $\pm 50\%$ regardless of the burn frequency. No probe polarization dependence was found for the holes and antiholes under either $[100]$ or $[110]$ burn polarization incident upon a $[100]$ -cut crystal.

4. DISCUSSION

In this study it has been found that hole burning is observed to occur only when the host is double-doped by the addition of a second alkali halide. This result can be explained by the following argument. The homogeneous width of SH^- is equal to half of the low-intensity short-burn-time hole width [see Eq. (4)] and is thus 0.021 cm^{-1} in KI + 2% KBr and 0.014 cm^{-1} in CsI + 2% RbI. It is reasonable to suppose that approximately the same values would hold for the singly doped hosts, just as was explicitly found to be true for $\text{CN}^-:\text{Na}^+$ compared with isolated CN^- by fluorescence measurements.⁵ Therefore, by inspection of Table 1, it follows that the lines in the singly doped hosts are almost homogeneously broadened (to within a factor of 2) and thus would not be expected to exhibit hole burning. It is necessary to inhomogeneously strain broaden the lines, by double-doping the hosts, in order to make PIRSH burning allowable.

This situation is analogous to that discovered previously for ReO_4^- (Ref. 1) and for CN^- .⁵ For ReO_4^- it was found that the main line could be burned, provided that it was strain broadened either by double-doping the host or by single-doping with a sufficiently high ReO_4^- concentration. For CN^- , in contrast, the main line was never ob-

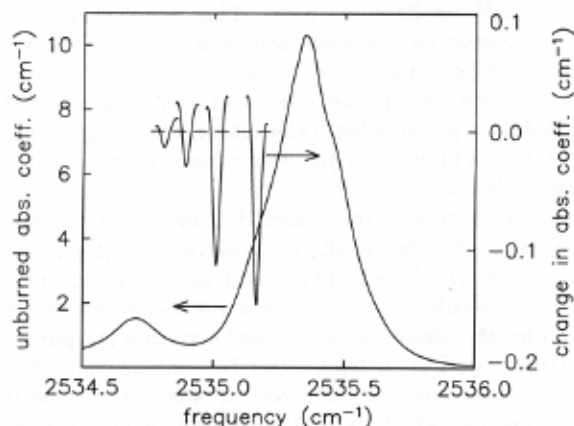


Fig. 6. Holes individually burned in the $^{32}\text{SH}^-:\text{Rb}^+$ and the main $^{32}\text{SH}^-$ vibrational modes. The main curve (left-hand axis) is the original, unburned FTIR spectrum from Fig. 5, and the overlaid curves (right-hand axis, with an expanded scale) show the holes and the edges of the antiholes resulting from burning at 2534.81 , 2534.89 , 2535.01 , and 2535.16 cm^{-1} for 1 min at 2 W/cm^2 .

Table 2. Observability of a Hole for a Given Defect Symmetry and Burn and Probe Polarizations

Defect Orientation	Burn Polarization	Probe Polarization	Hole Observable? ^a
$\langle 100 \rangle$	[100]	[100]	Y
		[010]	N
	[110]	[110]	Y
$\langle 111 \rangle$	[100]	[110]	Y
		[$\bar{1}\bar{1}0$]	Y
	[110]	[100]	Y
		[010]	Y
$\langle 110 \rangle$	[100]	[110]	Y
		[$\bar{1}\bar{1}0$]	N
		[100]	Y
	[110]	[010]	Y
		[110]	Y
		[$\bar{1}\bar{1}0$]	Y

^aY indicates that a hole may be observed for this choice of polarizations, and N indicates that holes cannot be seen.

served to burn; however, a neighboring line, attributed to a $\text{CN}^-:\text{Na}^+$ combination (that is to say, with a substitution for a 1nn K^+ atom by a Na^+ atom), could be burned. In the present study it has been found that the strain-broadened main line can be burned, as can a neighboring line, which has been attributed to a SH^- ion combination.

The models that are proposed to explain the hole-burning mechanisms for ReO_4^- and for CN^- are quite different from one other. An important question to ask is therefore, which one is better able to explain the present results for SH^- ? As is shown below, the answer is the model devised for ReO_4^- , but with a couple of necessary modifications.

To begin with, it is reasonable to assume that the SH^- hole burning proceeds by reorientation of the molecule, since this mechanism has been proposed for all previous PIRSH studies in alkali halides: ReO_4^- ,¹ NO_2^- ,^{3,4} and CN^- .⁵ In that case the polarization results indicate that for the SH^- center in KI + 2% KBr the reorientation must proceed by 180° head-to-tail flips of the center. The proof involves a consideration of both the hole and the antihole polarization dependences.

First, the polarization of the hole indicates a $\langle 111 \rangle$ orientation for SH^- in KI + 2% KBr. This implication can be seen by correlating the observations at the end of Subsection 3.A.2 with Table 2, which lists under what combinations of burn and probe polarizations a hole can be observed for a given defect orientation, assuming that the electric dipole moment of the defect lies parallel to its orientation; that is to say, in this case, it lies along the line joining the centers of the S and H atoms. This orientation agrees with the results of stress measurements¹³ on singly doped KI. It is emphasized that the orientation of the SH^- molecule is $\langle 111 \rangle$ even when it has a 2nn Br^- defect. The SH^- dipole does not bend over into the particular $\langle 110 \rangle$ direction in which the Br^- ion is located, in contrast to the case for $\text{CN}^-:\text{Na}^+$; it was found⁵ that the CN^- molecule, which is $\langle 111 \rangle$ oriented in singly doped KBr, reorients into the $\langle 100 \rangle$ direction, along which the Na^+ atom resides. Of course these two centers are not exactly analogous in any case, because the Br^- substitution occurs farther from the SH^- defect than does the Na^+ from CN^- , namely, on a 2nn, not a 1nn, site. However,

even for the $\text{SH}^-:\text{Rb}^+$ center in CsI, where the substitution now occurs on a 1nn site, the dipole is not oriented along the $\langle 111 \rangle$ direction connecting the SH^- site to the Rb^+ atom. Instead the polarization of the hole indicates a $\langle 110 \rangle$ defect orientation.

Second the polarization of the antihole for the SH^- center in KI + 2% KBr is found to be the same as that of the hole. In particular no antihole is found for [110] burn and [$\bar{1}\bar{1}0$] probe polarization. This implies that the hole-burning mechanism cannot proceed by reorientation between adjacent $\langle 111 \rangle$ potential wells. Only 180° head-to-tail reorientations are consistent with the requirement that the polarization dependence of the defect be unchanged before and after hole burning. It may be that this restriction to 180° reorientations arises from relaxation of the host atoms surrounding the SH^- dipoles. In the case of CsI + 2% RbI it is not possible to determine how the SH^- dipole is reorienting during hole burning, since an antihole is observed for every combination of burn and probe polarizations, owing to the $\langle 110 \rangle$ defect orientation. For the sake of simplicity, however, it is assumed that the reorientation proceeds by 180° head-to-tail flips in this case also.

One last piece of information is important before a microscopic model for the SH^- hole-burning mechanism can be proposed. This information concerns the location of the antihole relative to that of the hole. For both the SH^- ion band and the main SH^- line (in KI + 2% KBr and in CsI + 2% RbI), the antihole absorption lies within a few homogeneous widths of the hole, at both higher and lower frequencies, and is significantly broader than the hole. This situation is to be contrasted with that for $\text{CN}^-:\text{Na}^+$, where the antihole appeared in a different absorption band than did the hole, 5.9 cm^{-1} (177 GHz) removed in frequency from it.⁵ The difference in the SH^- stretching frequencies in the original and the burned orientations is small and is distributed over a range of positive and negative values. This observation strongly suggests that the energy asymmetry for these two configurations arises from short-range randomly varying strain fields (or rather, strain gradients, in order to break the inversion symmetry at the SH^- sites) in the crystal, created by the presence of the 2 mol. % of size-mismatched alkali or halide ions.¹⁴

This idea, that the breaking of the configurational degeneracy arises from elastic strain gradients in the host, has been proposed previously¹ to explain the observation of PIRSH burning in ReO_4^- . Notice that in the cases of both ReO_4^- and SH^- the main line is found to exhibit hole burning only in the wings. A natural explanation can be suggested. Centers whose stretching frequencies lie in the wings of the lines must be experiencing the largest strains. (The singly doped boules presumably contain relatively weak internal strain fields. Thus, in the doubly doped samples, SH^- centers with stretching frequencies that coincide with those of the respective singly doped samples—that is, frequencies near the absorption peaks, as seen from Figs. 1 and 5—must be sitting at sites of low strain.) But the gradient of the strain field at some site in the crystal is approximately proportional to the magnitude of the strain at that location (and inversely proportional to the distance from the sources of strain, i.e., from the Br^- or Rb^+ ions). One thus expects only those centers

that lie in the wings of the main lines to burn holes, just as is observed.

Pulling together the various threads of reasoning developed in this section, we propose the following model for the hole-burning mechanism of SH^- :

1. Once in every 1700 times that a SH^- molecule is vibrationally excited, the molecule does not return to its original ground state but to a state in which it is flipped 180° .
2. It requires tens to hundreds of seconds for a flipped center in its vibrational ground state at 1.5 K to revert to its original orientation.
3. The stretching frequency of a SH^- molecule typically differs by plus or minus a few gigahertz in its flipped configuration, as compared with its original orientation, as a result of short-range strain gradients arising from the presence of neighboring alkali or halide ions, which have a different size than the host ions. Thus a hole and an antihole result when SH^- molecules flip over during vibrational deexcitation.

It is straightforward to develop an appropriate mathematical formalism for this model, patterned after the phenomenology developed in Ref. 1. This development is under way; preliminary results are encouraging.

5. CONCLUSIONS

Persistent infrared spectral holes have been burned, for the first time to our knowledge, in the fundamental stretching mode of SH^- doped in alkali halides by double-doping the host with a small amount (2 mol. %) of a second alkali halide. The key results obtained in the course of this study are the following:

1. The PIRSH's decay within tens to hundreds of seconds at 1.5 K, in contrast to the apparently permanent holes burned in strain-broadened ReO_4^- ,¹ in NO_2^- ,^{3,4} and in $\text{CN}^-:\text{Na}^+$.⁵
2. SH^- is $\langle 111 \rangle$ oriented in KI + 2% KBr and $\langle 110 \rangle$ oriented in CsI + 2% RbI, even for the SH^- :ion combinations.
3. The quantum efficiency for hole burning of SH^- in KI + 2% KBr is approximately 6×10^{-4} .
4. The energy relaxation times are found to be 250 ps for SH^- in KI and 370 ps in CsI.

5. Hole-burning proceeds by means of 180° head-to-tail flips of the SH^- molecule between orientations rendered inequivalent by short-range strain field gradients arising because of the double-doping of the crystal.

Future studies should focus on the nature of the local potential energy surfaces of the SH^- molecules: Why are the SH^- molecules restricted to 180° reorientations? What is the nature of the barrier between the two configurations? How do elastic strain gradients couple to the SH^- vibrations?

ACKNOWLEDGMENTS

Conversations with W. P. Ambrose, S. P. Love, U. Happek, and R. H. Silsbee were particularly helpful. This research has been supported by the National Science Foundation, grant DMR-89-18894, and by the U.S. Army Research Office, grants DAAL03-K-0053 and DAAL03-90-G-0040.

REFERENCES AND NOTES

1. W. E. Moerner, A. R. Chraplyvy, A. J. Sievers, and R. H. Silsbee, *Phys. Rev. B* **28**, 7244 (1983).
2. A. J. Sievers and W. E. Moerner, in *Persistent Spectral Hole-Burning: Science and Applications*, W. E. Moerner, ed. (Springer-Verlag, Berlin, 1988), Chap. 6.
3. W. P. Ambrose and A. J. Sievers, *Chem. Phys. Lett.* **147**, 608 (1988); *Phys. Status Solidi B* **151**, K97 (1988); *Phys. Rev. B* **38**, 10170 (1988).
4. W. P. Ambrose, J. P. Sethna, and A. J. Sievers, *J. Chem. Phys.* **95**, 8816 (1991).
5. R. C. Spitzer, W. P. Ambrose, and A. J. Sievers, *Phys. Rev. B* **34**, 7307 (1986).
6. The integral is taken over only the main line and does not include the sidebands of unknown origin that are observed at $\sim 100 \text{ cm}^{-1}$ higher and lower frequencies.
7. C.-K. Chi and E. R. Nixon, *J. Phys. Chem. Solids* **33**, 2101 (1972).
8. R. H. Silsbee, *J. Phys. Chem. Solids* **28**, 2525 (1967).
9. S. Völker, *J. Lumin.* **36**, 251 (1987).
10. L. R. Narasimhan, K. A. Littau, D. W. Pack, Y. S. Bai, A. Elschner, and M. D. Fayer, *Chem. Rev.* **90**, 439 (1990).
11. J. Friedrich and D. Haarer, *Angew. Chem. Int. Ed. Engl.* **23**, 113 (1984).
12. U. Happek, J. T. McWhirter, C. E. Mungan, and A. J. Sievers, *Bull. Am. Phys. Soc.* **36**, 918 (1991).
13. W. Kuch and U. Dürr, *J. Phys. Chem. Solids* **42**, 677 (1981).
14. A. M. Stoneham, *Rev. Mod. Phys.* **41**, 82 (1969).